UNIVERSITA' DEGLI STUDI DI NAPOLI

FEDERICO II

SCUOLA DI MEDICINA E CHIRURGIA

DIPARTIMENTO DI SCIENZE BIOMEDICHE AVANZATE

CORSO DI DOTTORATO DI RICERCA IN IMAGING MOLECOLARE

XXVI CICLO

COORDINATORE: PROF.MARCO SALVATORE

TESI DI DOTTORATO

Genetic Deletion in Uncoupling Protein 3 Augments 18F-Fluorodeoxyglucose Cardiac Uptake in the Ischemic Heart

RELATORE
Prof. Alberto Cuocolo

CANDIDATO
Dr.ssa Maria Piera Petretta

ANNO ACCADEMICO 2012/2013

INDEX

ABSTRACT

Background — Uncoupling protein 3 (UCP3) is a member of the mitochondrial anion carrier super-family of proteins expressed in the mitochondrial inner membrane that uncouple oxygen consumption by the respiratory chain from ATP synthesis. UCP3 plays a role in fatty acid metabolism and energy homeostasis and is required to maintain high rates of glucose aerobic metabolism, while deficiency in UCP3 might results in a metabolic shift that promotes anaerobic glycolytic metabolism. In this study, we investigated the effects of UCP3 genetic deletion on ^{18}F-fluorodeoxyglucose (FDG) cardiac uptake by a high-resolution positron emission tomography (PET)/computed tomography (CT) dedicated animal system after permanent coronary artery ligation.

Methods and Results — To test the effects of UCP3 genetic deletion in vivo, cardiac 18F-FDG PET/CT was performed in UCP3 knockout ($UCP3^{-/-}$) and wild-type (WT) mice one week after induction of myocardial infarction or sham procedure. In sham-operated mice no difference in left ventricular (LV) volume was detectable between WT and

UCP3$^{-/-}$. After myocardial infarction, LV volume was higher in both WT and UCP3$^{-/-}$ compared to sham animals, with a significant interaction ($P < 0.05$) between genotype and myocardial infarction. In sham-operated animals no difference in FDG standardized uptake value (SUV) was detectable between WT (1.8 ± 0.6) and UCP3$^{-/-}$ (1.8 ± 0.6). After myocardial infarction, SUV was higher in both WT (2.2 ± 0.6) and UCP3$^{-/-}$ (4.0 ± 0.9) compared to sham animals, with a significant interaction ($P < 0.005$) between genotype and myocardial infarction. A significant relationship ($r = 0.68$, $P < 0.001$) between LV volume and SUV was found.

Conclusions — In a mice model of permanent coronary occlusion, UCP3 is required to maintain high rates of glucose aerobic metabolism and its deficiency results in a metabolic shift that favored anaerobic glycolytic metabolism and increased FDG uptake.

INTRODUCTION

Cardiac positron emission tomography (PET) with deoxy-2[18F]fluoro-D-glucose (18F-FDG) is a nuclear medicine technique able to give unique insight into biochemical changes on a molecular level, with excellent sensitivity and has been increasingly used for non-invasive evaluation of myocardial pathophysiology in small animals (1). In the last years mice became the animals of choice in the pre-clinical research due to their short life cycle, and the possibility of genetic manipulation (2).The dimension of mice heart, with left ventricle wall thinner than 1 mm, represents a challenge for imaging acquisition and analysis in these animals, requiring expensive equipment capable of obtaining high-resolution images and established expertise (3). Good promising results have been achieved with PET (4) and with single-photon emission computed tomography (SPECT) (5,6) for rats and mice. Recently our group addressed the reproducibility of high-resolution PET/computed tomography (CT) system by repeated measurements in the same animals (7), to comprehensively evaluate the reproducibility of 18F-FDG for non-invasive quantification of infarct size in mice by a high-resolution animal PET/CT system. Heart failure (HF)

represents one of the main causes of death and mortality in the Western countries and this pathological condition is caractherized by molecular changes which result in altered trascritional leveles of key enzymes and proteins. In particular, Uncoupling protein 3 (UCP3), a member of the mitochondrial anion carrier expressed in the mitochondrial inner membrane that uncouple oxygen consumption by the respiratory chain from ATP synthesis, seems to be involved in the adaptive modifications of the failing heart (8). Patients with heart failure also have elevated plasma free fatty acid (FFA) concentrations. Elevated FFA levels are associated with increased cardiac mitochondrial uncoupling proteins (UCPs), which, in turn, are associated with decreased mitochondrial respiratory coupling and low cardiac efficiency. UCP3 plays a role in fatty acid metabolism and energy homeostasis and is required to maintain high rates of glucose aerobic metabolism, while deficiency in UCP3 might results in a metabolic shift that promotes anaerobic glycolytic metabolism. In this study, we investigated the effects of UCP3 genetic deletion on 18F-FDG uptake by PET/CT dedicated animal system after the induction of myocardial infarction (MI) by permanent coronary artery ligation.

- **Role of molecular imaging**

The universal definition of molecular imaging, as aprroved by tha task force recommended and the MICoE and SNM boards is the following: "Molecular imaging is the visualization, characterization, and measurement of biological processes at the molecular and cellular levels in humans and other living systems" (9). E.A. Zerhouni, former director of the National Institutes of Health, has described molecular imaging as having "…the potential to define itself as a core interdisciplinary science for extracting spatially and temporally resolved biological information at all physical scales from Angstroms to microns to centimeters in intact biological systems" (10).This biomedical research discipline allows the early identification of biologic processes underlying pathological conditions at cellular and subcellular levels, before of clinical manifestations. Actually many diseases are identified only after the appearance of symptoms. Conventional imaging techniques allows the diagnosis of diseases sometimes in an advanced stage; so to restrain the evolution of disease and to avoid the relentless progression, we need to recognize it in a very early stage. Molecular imaging allows the

identification of cellular and molecular pathways and mechanisms of disease present in the living subject. In this way, biologic processes can be studied not in vitro or ex vivo biopsy/cell culture laboratory techniques, but in their own physiologically environment. Molecular imaging constis of multiple image-capture techniques and can be performed with a range of instruments, with a specific region of the electromagnetic spectrum including magnetic resonance imaging (MRI), x-ray computed tomography (CT), positron emission tomography (PET), single photon emission computed tomography (SPECT), and optical (bioluminescence and fluorescence imaging). New imaging instruments were designed and fabricated with the purpose of advancing the use of small research animals in molecular imaging studies through the use of dedicated imaging instruments with high sensitivity and resolution. Moreover, dual modality, as hybrid PET/CT scanners, have become the refernce tool for nuclear medicine, and dedicated PET/CT and SPECT/CT scanners for small animal imaging are now used routinely. The advantages of these integrated instruments derives from the possibility of combining functional imaging strength of one technology, such as PET and SPECT, with the high resolution anatomical imaging afforded by MRI or CT. The various

imaging technologies differ in many aspects such as depth penetration, spatial resolution, energy expended for image generation, availability of injectable/biocompatible molecular probes and the respective detection threshold of probes for a given technology. PET, in particular, is a nuclear medicine technique for in vivo evaluation of molecular events, quantification of metabolic functions in organs and tissues and it is currently used for diagnosis and assessment of therapy response. In the last decades nuclear medicine techniques are widely used also in preclinical field. In particular small animal PET tomographs, with an improved low spatial resolution (that reaches 1 mm), permit macroscopic visualization of cellular processes and give the possibility of longitudinally following the development of the disease or the response to a specific new therapy overtime and in the same subject reducuing the number of animals employed (11). Moreover preclinical PET imaging could be defined a "translational imaging" because of employing the same technology in an experimental setting and in clinical practice. MRI also is used in pre-clinical studies, with the advantage of higher spatial resolution and the ability to extract physiologic and anatomic information simultaneously. Molecular imaging allows to visualize, characterize and quantify normal

and pathologic processes at the cellular and subcellular level by molecular targets. The choice of target is generally based on key molecules, such as specific cell surface markers, genes or gene products that are specifically associated with a particular physiologic or pathologic process. In particular, genomics and proteomics have developed techniques to identify genes involved in disease processes, and specific proteins that are structurally abnormal or that are expressed at abnormally high or low levels in a disease state. In the last decades, molecular imaging is a rapidly growing with the potential to elucidate biological processes at the cellular and molecular levels, and to translate scientific discoveries in the research laboratory into the clinical setting. Data derived from preclinical assestment and their translation into clinical trials promises to accelerate the development of individualized therapies tailored to a patient's genetic composition. Molecular imaging offers unique insights that allow a more personalized approach to evaluation and management of cardiovascular diseases, such as: ischemic injury, heart failure, and left ventricular remodeling; thrombosis, atherosclerosis, and vulnerable plaque; angiogenesis, transplant rejection, and arrhythmic substrates.

- **Cardiovascular diseases and their pathological basis.**

Cardiovascular diseases, such as Coronary Heart Disease (CHD) represent a leading cause of morbidity and mortality in the western countries and a relevant cause of permanent disability, myocardial infarction and congestive heart failure (12). Despite several progression in diagnosis and treatment of coronary artery diseases and myocardial ischemia, there is a growing interest for the study of cardiac metabolism as a potential target for the treatment of cardiovascular diseases. A reduced cardiac energy status, which decreases the functional capacity of the myocardium, is associated with heart failure (13). Chronic changes in cardiac metabolism are supported by trascritional alterations which consist in the swicht from the prevalent oxidation of fatty acids to glucose oxidation. This alterated metabolic status is sometimes associated with changes in trascritional levels of different key enzymes, such as Uncoupling Protiens (UCPs), a family of anion carrier proteins localized at the level of the mitochondrial inner membrane where they plays a role in mitochondrial energy metabolism as well as reactive oxygen species (ROS) generation (14). These proteins catalyze a regulated proton leak across the mitochondrial

inner membrane, diverting free energy from the ATP synthesis chain to the production of heat (15) and thus reducing reactive oxygen species production (16) (Figure 1). So far, 5 UCP isoforms have been identified in mammals, named UCP1 to 5 in order of their discovery (17). UCP1, the first isoform discovered, is primarily expressed in the brown adipose tissue, where it dissipates the energy potential generated by respiration to serve both thermoregulatory and metaboregulatory roles (18). UCP2 is present in many organs and cell types, and UCP3 is predominantly expressed in skeletal muscle; different from UCP1, they do not contribute to adaptive thermogenesis but may be involved in the resting metabolic rate (19). In particular both UCP2 and UCP3 seem to be involved int the control of reactive oxygen species levels and regulation of fatty acid metabolism, whereas UCP2 only seems to control insulin secretion (20) and UCP3 is probably involved in fatty acid metabolism in skeletal muscle and heart (21).

UCP3 is also involved in regulation of fatty acid metabolism, adaptive responses to acute exercise and prevention of reactive oxygen species (ROS) formation. To address these questions, Vidal-Puig et al. have generated a transgenic murine model lacking UCP3 (UCP3 knockout

mice) and in this transgenic murine model they have found that skeletal muscle mitochondria are more coupled and that ROS production is increased (22). We know that in the failing heart there is an alterated metabolic state characterized, for example, by an enhanced mitochondrial ROS production which contributes to the alterated cardiomyocytes function (23,24). Under normal conditions, cardiac muscle satisfies its high-energy requirements by oxidizing fatty acids (FAs) and carbohydrates and, to a lesser extent, amino acids. The failing heart, instead, looses its metabolic flexibility and relies more on glucose as its preferential substrate. UCP3 in particular acts as a fatty acid anion transporter, to protect from lipid peroxidation (25). When fatty acid supply is high, a larger fraction of fatty acid enters the matrix via a transmembrane fatty acid flip-flop mechanism; the imported fatty acid would be nonmetabolized and accumulated because of the lack of matrix acyl-CoA synthases (26). Accumulation of fatty acid in the matrix increases the risk of mitochondrial lipid peroxidation, which may be toxic. UCP3-mediated fatty acid efflux would protect against such damage. Moreover, a positive correlation between fasting plasma-free-fatty acid concentrations and cardiac UCP3 protein levels has been found in patients suffering from

heart failure (21). UCP3 is also expressed in cardiac muscle, where its role remains relatively unexplored and it is controversial if it plays a beneficial or detrimental role in heart failure development (27). Actually it has been suggested that under hypoxic conditions, mitochondria can damage cardiomyocytes generating toxic reactive oxygen species (ROS) and that cardiac UCP3 activation attenuates ROS production (28) and related cellular damage in myocardial areas of acute or chronic ischemia and upon reperfusion (29). At the same time, UCP3 up-regulation could have a detrimental effect in heart failure progression, contributing to energy deficit and reduced cardiac efficiency, via uncoupling mitochondrial respiration (30). Animal models over- or under-expressing UCP3, evaluated by ex vivo genomic or proteomic analysis, did not provide uniform answers. Increased mitochondrial uncoupling, affecting total ATP synthesis rates, could be an important candidate to explain this decreased cardiac energy status. Given the presence of UCP3 in cardiac tissue, it can be postulated that an increased UCP3-mediated uncoupling contributes to the observed energy deficit in cardiac tissue during heart failure. Animal models are currently used to understand in vivo the pathophysiological mechanism causing heart diseases and to improve

diagnosis and therapeutic strategies. At the same time, dedicated high resolution small animal imaging has acquired a critical role in rodent cardiac studies, replacing ex vivo techniques such as histology, autoradiography and radiation counting of tissue samples. Positron Emission Tomography (PET), in particular, is a successful tool to study non invasively, quantitatively and repeatedly, gene expression involved in myocardial energetic metabolism, apoptosis, angiogenesis, hypoxia, inflammation, and to measure infarct size, a relevant clinical objective for early monitoring the response to innovative molecular therapies. Nevertheless, serial assessment of morphometric changes are also relevant in the evaluation of left ventricular (LV) pathophysiology. Therefore, assessment of LV geometry, in addition to biochemical properties of the myocardium, within the same PET would be highly desiderable, because it obviates the need for a second imaging modality (31,32). Association with X-ray Computed Tomography (micro-CT) adds high resolution anatomical information, allowing a fine spatial localization of the radiotracer biodistribution.

AIM OF THE WORK

In this study we used in vivo 18F-FDG PET/CT to assess myocardial viability, to quantify heart glucose metabolism and to measure infarct size in a mouse model lacking UCP3. We also evaluated a novel method for the additional quantification of LV volumes and total surface area working on polar maps obtained by static and nongated 18F-FDG PET datasetwith the purpose of evaluate potential utility of 18F-FDG PET/CT to highlight alterations in myocardial energetic metabolism and morphology.

MATERIALS AND METHODS

- **Animal studies**

Animal experiments conformed to the "Guide for the Care and Use of Laboratory Animals" published by the US National Institutes of Health (NIH Publication No. 85-23, revised 1996) and were approved by the animal welfare regulation of University Federico II of Naples, Italy. Mice were purchased from the Jackson Laboratory (genetic background-strain: 129S4/SvJae). The $UCP3^{-/-}$ mice were obtained as previously described (22). Male adult $UCP3^{-/-}$ (aged 8 to 9 weeks, n=17) and WT mice (aged 8

to 9 weeks, n=14) were included in the study and maintained under identical conditions of temperature (21±1°C), humidity (60±5%), and light–dark cycle and had free access to normal mouse chow.

- **Mouse model of myocardial infarction**

Myocardial infarction was induced in UCP3$^{-/-}$ (n=8) and WT mice (n=8) by permanent ligation of the eft coronary artery. Sham-operated animals underwent the same procedure without ligation of the left coronary artery at the same time (sham: WT n=6 and UCP3$^{-/-}$ n=9). Permanent ligation of left coronary artery was performed as previously described (33) using a surgical microscope to clearly detect and ligate the small vessel, dedicated microsurgical instruments, thin sutures and needles, and a customized mouse ventilator (Harvard Apparatus, March-Hugsstetten, Germany). Briefly, mice were anesthetized with 2.4% sevofluorane plus oxygen, fixed in a supine position on a heating table to prevent hypothermia, intubated and ventilated with a tidal volume of 200 µl and a respiratory rate of about 110 breaths/min. The toracotomy was performed by a trasverse 5 mm incision of the left fifth intercostal space, 2 mm away from the left sternal border, then the pericardial sac was opened and the left

anterior descending coronary artery (LAD) was occluded 2–3 mm distal to the tip of the left auricle using a 7.0 silk suture.

- **Trans-thoracic echocardiography**

Trans-thoracic echocardiography was performed 7 days (range 5-8) after surgery in both myocardial infarction and sham groups using the Vevo 770 high-resolution imaging system (VisualSonics), as previously described (34). Briefly, mice were anesthetized with an intramuscular injection of ketamine 100 mg/kg and xylazine 2.5 mg/kg, and echocardiograms were performed with a 30-MHz RMV-707B scanning head. Cardiac function was evaluated by measuring LV fractional shortening.

- **Protocol for PET/CT studies**

The accuracy and reproducibility of high-resolution positron emission tomography/computed tomography with 2-deoxy-2 [18F]fluoro-D-glucose (18F-FDG) for noninvasive quantification of myocardial infarct size in mice have been recently documented (7). The same day of echocardiography, PET/CT was performed in all mice using a dedicated

animal PET/CT scanner (dual ring version)(eXplore Vista, GE Healthcare, Milwaukee, WI, USA) with an axial field of view (FOV) of 4.8 cm and a transaxial FOV of 6.7 cm. PET radial spatial resolution was of 1.6 mm full-width at half maximum and a CT spatial resolution of 200 μm. Proprietary software permitted to perform PET/CT co-registration and semi-quantitative analysis of PET dataset. The animals had unrestricted access to water and their normal food before scanning. Prior to imaging, mice were warmed for 15 minutes with an infrared lamp to induce vasodilatation of the lateral tail vein, then anesthetized with a mixture of isoflurane 4% and oxygen 1 L/minute for 5 minutes and positioned in the mouse restrainer. A dose of 300 MBq/kg of ^{18}F-FDG was administrated as a bolus in the lateral tail vein by a 30-gauge needle (injection volume, 100 μl). Animals were maintained at a temperature of 23°C during the biodistribution of FDG. After 40 minutes, mce were anesthetized with ketamine 100mg/kg and xylazine 10 mg/kg (injection volume, 100 μl/10g). Thereafter, the mice, with the heart centered in the tomograph, were symmetrically positioned on a warm bed with micropore tape, and a 15-minute static PET (single bed position with an axial field-of-view of 4.8 cm; energy window 250-700 keV) scan was performed, followed by a

7-minute CT scan. This standardized procedures improved animal welfare and heart visualization with FDG, avoiding stress for restrain or cold to reduce interscapular brown fat and and improve the uptake in the target structure.

- **Images analysis**

PET/CT images were processed as previously described (7). PET data were reconstructed using a 3D-FORE/2D-OSEM iterative algorithm (16 subsets, 2 iterations, matrix size 175 × 175, voxel size of 0.3875 × 0.3875 × 0.7750 mm^3) including random, scatter correction, dead time, decay, and attenuation correction using CT data. Reconstructed images were reoriented to obtain axial sections perpendicular to the left ventricle long axis and the whole ventricle wall was manually segmented tracing a region of interest in each slice (eXplore Vista Software). FDG myocardial uptake was measured in the left ventricle wall volume and expressed as standardized uptake value (SUV): tissue activity (MBq/cc)/[injected dose (MBq)/body weight (g)]). Automated image analysis software (MunichHeart) was used to measure left ventricle volume and infarct size on the basis of volumetric sampling of tracer uptake (35). This software

allowed long-axis definition, volumetric polar map calculation, and report page generation for the database. Each polar map was normalized to its maximum uptake value. Extent of infarct was expressed in percentage value (% defect area/LV area) by counting the elements in the polar map with an activity below a threshold (50% of the maximum) and relating this value to the total number of polar map elements. The reproducibility and accuracy of this approach for measurement of infarct size in a mice model of permanent coronary occlusion have been documented (7)

- **Histology**

Twenty mice (16 of MI group and 4 of sham group) were killed immediately after the PET/CT scan to perform histological analysis. Hearts were arrested in diastole with a 300-lL injection of saturated KCl solution in the right atrium and then excised. The heart was excised and immersed into 10% buffered formalin solution for 24 hours. After being kept for more than 2 days in 10% buffered formalin solution, the whole left ventricle was embedded in paraffin. Transverse serial sections 20-µm thick were cut, and every 50th section from the apex to the base (every 1 mm) was mounted and stained with Masson's trichrome. Between five and

seven slides were obtained from each heart and photographed and analyzed morphometrically. Calibrated and magnified digital photographs were analyzed planimetrically using Java-based image processing program (ImageJ, National Institutes of Health, Bethesda, MD). The midmyocardial contour of the viable LV wall and the extent of scarred myocardium were traced on each image. Measurements from the slides were averaged and infarct size was expressed as a percentage of scar tissue to total left ventricular area (36).

- **Statistical analysis**

All data were expressed as mean ± standard deviation. Comparisons between two groups were performed using the unpaired Student t test. Two-way analysis of variance was performed to analyze differences by genotype and myocardial infarction among the four groups, including a Tukey post-hoc analysis if a significant F test occurred. Linear regression analysis was performed to evaluate the relationship between LV volume and SUV. A p value <0.05 was considered statistically significant.

RESULTS

Individual values of LV volume in the four groups of mice are illustrated in Figure 1. In sham-operated mice no difference was detectable between WT (56.1 ± 6.1 μl) and UCP3$^{-/-}$ (58.7 ± 5.1 μl). After myocardial infarction, LV volume was higher in both WT (59.9 ± 9.3 μl) and UCP3$^{-/-}$ (75.5 ± 10.8 μl) compared to sham animals, with UCP3$^{-/-}$ mice showing the highest values. At two-way analysis of variance a significant interaction ($P < 0.05$) between genotype and myocardial infarction was found (Table 1).

At trans-thoracic echocardiography, sham-operated UCP3$^{-/-}$ mice showed LV fractional shortening comparable to WT (56.5 ± 4.6% and 54.1 ± 4.2%, respectively, P = NS). After myocardial infarction, LV fractional shortening was significantly lower ($p < 0.05$) in both WT (42.7 ± 3.1%) and UCP3$^{-/-}$ (24.4% ± 2.5%) mice compared to sham-operated animals. UCP3$^{-/-}$ mice displayed a significant worsening in cardiac function after coronary artery ligation compared with WT ($P < 0.05$). Furthermore, UCP3 genetic deletion increased infarct size after coronary artery ligation as compared to WT (44 ± 9% vs. 29 ± 7%, P <0.005). Vertical long-axis,

horizontal long-axis, and short-axis slices and the resulting polar map in a WT mouse and an UCP3$^{-/-}$ mouse after myocardial infarction are illustrated in Figure 2.

Figure 3 shows individual values of SUV in the four groups of mice. In sham-operated animals no differences were detectable between WT (1.8 ± 0.6) and UCP3$^{-/-}$ (1.8 ± 0.6). After myocardial infarction, SUV was higher in both WT (2.2 ± 0.6) and UCP3$^{-/-}$ (4.0 ± 0.9) compared to sham animals, with UCP3$^{-/-}$ mice showing the highest values. The results of two-way analysis of variance are reported in Table 2. As shown, a significant interaction ($P < 0.005$) between genotype and myocardial infarction was found. Finally, at linear regression analysis a significant relationship ($r=0.68$, $P < 0.001$) between LV volume and SUV was found (Figure 4).

DISCUSSION

In this study we investigated the role of UCP3 protein in cardiac remodelling and heart failure progression in wild type and UCP3$^{-/-}$ mice models of myocardial infarction. We evaluated alterations in myocardial energetic metabolism related to UCP3 expression by in vivo 18F-FDG PET imaging. Moreover, we quantified non invasively left ventricle geometrical parameters such as total surface area and volume by Munich Heart software for the first time. This study demonstrates that after permanent coronary artery ligation UCP3 genetic deletion is associated with higher cardiac FDG uptake, larger infarct size and remodeling as compared to WT mice. These findings suggest that UCP3 deletion induces a metabolic shift that favored anaerobic glycolytic metabolism. Moreover, the larger area of necrosis and remodeling in response to ischemia in mice leaking UCP3 confirms the cardioprotective role of this protein. 18F-FDG PET is considered a gold standard in identifying patients with coronary artery disease and left ventricular dysfunction (37) with the clear advantage to provide serial measurements over time, useful to monitor the

evolution of a disease or the response to a treatment. The failing myocardium is characterized by changes in energy and substrate metabolism, that could reflect an increased energy demand and/or a compromised capacity to generate sufficient amounts of ATP (38). Under normal conditions, the oxidation of fatty acids and glucose covers approximately 65% and 30% of cardiac energy demand, respectively. The significance of the metabolic shift from fatty acids towards glucose in failing myocardium is still being debated whether it should be considered adaptive or maladaptive. Various biochemical and genomic mechanisms have been involved in the alterations of energy metabolism in failing heart (30). It has been postulated that mitochondrial efficiency can be reduced due to the increased activity of UCPs, which may dissipate part of the mithocondrial proton gradient used to generate ATP. However, the exact biological function of UCP3 is already not clear and seems to be involved in mithocondrial uncoupling, export of fatty acids out of the mitochondrial matrix and inhibition of ROS production (39, 50) (Figure 5) . Both increases and decreases in UCP2 and UCP3 expression were reported in animals and patients with congestive heart failure (40, 41). UCP3 was required to maintain high rates of glucose aerobic metabolism, while

deficiency in UCP3 resulted in a metabolic shift that favoured anaerobic glycolytic metabolism, and increased glucose uptake (42). Mouse models in which UCP3 is overexpressed have reduced fat stores and are resistant to diabetes induced by dietary modifications, while knockout are obese and predisposed to type 2 diabetes and show increased sensitivity to oxidative damage in the muscle. Currently there are limited data on the UCP3 activity in the heart. In basal conditions there aren't significant differences in the mitochondrial membrane potential between wild type and $UCP3^{-/-}$. Thyroid hormones or fasting induce an increased expression of UCP3 in the heart (30). In patients with heart failure, the increased expression of UCP3 is related to a state of energy deficit infarction (21). The positive correlation between overexpression of UCP3 in heart failure and the rate of plasma non-esterified fatty acids (Free fatty acids, FFAs) suggests a primary role of UCP3 in the metabolism of fatty acids, similarly to the skeletal muscle. The increased cardiac expression of UCP3 in the course of heart failure would increase the transport of fatty acids across the mitochondrial membranes, protecting the mitochondria by the action toxic due to the accumulation of these anions (30). Furthermore, in case of ischemia and reperfusion, the mitochondria produce "reactive oxygen

species" (ROS) that can damage the cardiomyocytes. UCP3 is expressed in response to an ischemic insult, activating a mechanism cytoprotective antioxidant, as it is capable of reducing the production of ROS and subsequent reperfusion injury. Therefore, this protein is potential therapeutic target for the management of CHD (29). In rats it has been shown that the expression of UCP3 is inversely associated with infarct size, probably by activating a protective mechanism to prevent the death of cardiomyocytes in the tissue surrounding the infarcted area (43). Several PET clinical studies reported depressed fatty acids utilization in various forms of cardiomyopathy (44-47). Decreased, unchanged and increased cardiac deposition of FDG has been reported in the human failing heart; likewise autoradiography studies in cardiac hypertrophy rat model revealed that the cardiac uptake of radiolabelled fatty acids analogues was diminished and the uptake of FDG was enhanced (48). PET FDG uptake in skeletal muscles confirmed this findings in $UCP3^{-/-}$ and wild type mice (49). In this study we found that after permanent coronary artery ligation, infarct size and LV volume were significantly greater in $UCP3^{-/-}$ group compared to WT mice. Infarct size is one of the major determinants of post-ischemic cardiac remodeling and adverse outcome. To evaluate

cardiac function in WT and UCP3$^{-/-}$ mice after myocardial infarction, transthoracic echocardiography was performed in all experimental groups. Sham-operated UCP3$^{-/-}$ mice showed LV fractional shortening comparable to WT. After myocardial infarction, LV fractional shortening was significantly lower compared to sham-operated mice in both WT and UCP3$^{-/-}$ mice. Moreover, UCP3$^{-/-}$ mice displayed a significant worsening in cardiac function after coronary artery ligation compared with WT. Mailloux et al. (49) demonstrated that deficiency in UCP3 resulted in a metabolic shift in skeletal muscles that favored anaerobic glycolytic metabolism, increased glucose uptake and increased sensitivity to oxidative challenge and these findings were confirmed by FDG uptake at PET imaging. To explore whether this metabolic shift towards glycolysis is present also in cardiac muscle, we measured glucose uptake by monitoring myocardial FDG uptake in UCP3$^{-/-}$ and in WT mice with and without coronary artery ligation. Our results show no differences in sham-operated animals between WT and UCP3$^{-/-}$. On the other hand, after myocardial infarction SUV was higher in both WT and UCP3$^{-/-}$ compared to sham animals. Noteworthy, UCP3$^{-/-}$ mice showed the highest value of SUV and the results of two-way analysis of variance demonstrated a significant

interaction between genotype and myocardial infarction. We also found a significant relationship between LV volume and SUV. This finding indicates that adverse remodeling and metabolic derangement are direct related and that UCP3 deletion has an unfavorable impact on both parameters.

CONCLUSIONS

In his study we demonstrate, for the first time that, in a mice model of permanent coronary occlusion, UCP3 is required to maintain high rates of glucose aerobic metabolism and its deficiency results in a metabolic shift that favored anaerobic glycolytic metabolism and increased FDG uptake. Moreover we found a negative remodelling of the left ventricle in response to ischemia in mice leaking UCP3, confirming the cardioprotective role of this protein.

REFERENCES

1. Higuchi T, Nekolla SG, Jankaukas A, Weber AW, Huisman MC, Reder S, et al. Characterization of normal and infarcted rat myocardium using a combination of small-animal PET and clinical MRI. J Nucl Med 2007;48:288-94.
2. Klocke R, Tian W, Kuhlmann MT, Nikol S. Surgical animal models of heart failure related to coronary heart disease. Cardiovasc Res. 2007;74:29-38.
3. Ratering D, Baltes C, Do¨rries C, Rudin M. Accelerated cardiovascular magnetic resonance of the mouse heart using gnetic resonance of the mouse heart using self-gated parallel imaging strategies does not compromise accuracy of structural and functional measures. J Cardiovasc Magn Reson 2010;12:43-55
4. Kudo T, Fukuchi K, Annala AJ, Chatziioannou AF, Allada V, Dahlbom M, et al. Noninvasive measurement of myocardial activity concentrations and perfusion defect size in rats with a new small-animal positron emission tomograph. Circulation 2002;106:118-23.
5. Liu Z, Kastis GA, Stevenson GD, Barrett HH, Furenlid LR, Kupinski

MA, et al. Quantitative analysis of acute myocardial infarct in rat hearts with ischemia-reperfusion using a high-resolution stationary SPECT system. J Nucl Med 2002;43:933-9.

6. Wu MC, Gao DW, Sievers RE, Lee RJ, Hasegawa BH, Dae MW. Pinhole single- photon emission computed tomography for myocardial perfusion imaging of mice. J Am Coll Cardiol 2003;42:576-82.
7. Greco A, Petretta MP, Larobina M, Gargiulo S, Panico M, Nekolla SG, Esposito G, Petretta M, Brunetti A, Cuocolo A. Reproducibility and accuracy of non-invasive measurement of infarct size in mice with high-resolution PET/CT. J Nucl Cardiol. 2012-19(3):492-9.
8. Murray AJ, Cole MA, Lygate CA, Carr CA, Stuckey DJ, Little SE, Neubauer S, Clarke K. Increased mitochondrial uncoupling proteins, respiratory uncoupling and decreased efficiency in the chronically infarcted rat heart. J Mol Cell Cardiol. 2008 Apr;44(4):694-700.
9. The Journal of Nuclear Medicine • Vol. 48 • No. 6 • June 2007 - Dave Mankoff, MD, PhD Chair, Definitions Task Force.
10. Eugene P. Pendergrass New Horizons Lecture, Radiological Society of North America meeting, 2007- 1.Cited in J Nucl Med; 49:25N-26N,

2008.

11. Wang Y, Seidel J, Vaquero JJ, Pomper MG. Performance evaluation of the GE healtcare eXplore VIST dual-ring small-animal PET scanner. J Nucl Med 2006;47:1891-900.
12. Mosterd A, Hoes AW. Clinical epidemiology of heart failure. Heart. 2007;93:1137-1146.
13. Taegtmeyer H, Wilson C R, Razeghi P and Sharma S. Metabolic energetics and genetics in heart. Ann N.Y.Acad.Sci.1047:208-218. 2005.
14. MacLellan JD, Gerrits MF, Gowing A, Smith PJ, Wheeler MB, Harper ME. Physiological increases in uncoupling protein 3 augment fatty acid oxidation and decrease reactive oxygen species production without uncoupling respiration in muscle cells. Diabetes. 2005;54:2343-50.
15. Brand MD, Affourtit C, Esteves TC, Green K, Lambert AJ, Miwa S, Pakay JL, Parker N. Mitochondrial superoxide: Production, biological effects, and activation of uncoupling proteins. Free Radic Biol Med. 2004;37:755-767.
16. Casteilla L, Rigoulet M, Penicaud L. Mitochondrial ROS

metabolism: Modulation by uncoupling proteins. IUBMB Life. 2001;52:181-188.

17. Bezaire V, Seifert EL, Harper ME. Uncoupling protein-3: clues in an ongoing mitochondrial mystery. FASEB J. 2007;21:312–324.
18. Parker N, Crichton PG, Vidal-Puig AJ, Brand MD. Uncoupling protein-1 (UCP1) contributes to the basal proton conductance of brown adipose tissue mitochondria. J Bioenerg Biomembr. 2009;41:335–342.
19. Rousset S, Alves-Guerra MC, Mozo J, Miroux B, Cassard-Doulcier AM, Bouillaud F, Ricquier D. The biology of mitochondrial uncoupling proteins. Diabetes 53; S130-135, 2004.
20. Fleury C, Neverova M, Collins S, et al. Uncoupling protein-2: a novel gene linked to obesity and hyperinsulinemia. Nat Genet.1997;15:269-272.
21. Murray AJ, Anderson RE, Watson GC, Radda GK, Clarke K. Uncoupling proteins in human heart. Lancet. 2004;364:1786-88.
22. Vidal-Puig AJ, Grujic D, Zhang CY, Hagen T, Boss O, Ido Y, Szczepanik A, Wade J, Mootha V, Cortright R, Muoio DM, Lowell BB. Energy metabolism in uncoupling protein 3 gene knockout mice.

J Biol Chem. 2000 May 26;275:16258-66.

23. Ide T, Tsutsui H, Kinugawa S, et al. Direct evidence for increased hydroxyl radicals originating from superoxide in the failing myocardium. Circ Res. Feb 4 2000;86(2):152-157.

24. Ruffolo RR, Jr., Feuerstein GZ. Neurohormonal activation, oxygen free radicals, and apoptosis in the pathogenesis of congestive heart failure. J Cardiovasc Pharmacol. 1998;32 Suppl 1:S22-30.

25. Schrauwen, P., Saris, W. H., and Hesselink, M. K. An alternative function for human uncoupling protein 3: protection of mitochondria against accumulation of nonesterified fatty acids inside the mitochondrial matrix. FASEB J.(2001) 15, 2497–2502.

26. Skulachev, V. P. Fatty acid circuit as a physiological mechanism of uncoupling of oxidative phosphorylation. FEBS Lett. 1991;294, 158–162.

27. Ljubicic V, Adhihetty PJ, Hood DA. Role of UCP3 in state 4 respiration during contractile activity-induced mitochondrial biogenesis. J Appl Physiol (1985). 2004;97:976-83.

28. Perrino C, Schiattarella GG, Sannino A, Pironti G, Petretta MP, Cannavo A, Gargiulo G, Ilardi F, Magliulo F, Franzone A, Carotenuto

G, Serino F, Altobelli GG, Cimini V, Cuocolo A, Lombardi A, Goglia F, Indolfi C, Trimarco B, Esposito G. Genetic deletion of uncoupling protein 3 exaggerates apoptotic cell death in the ischemic heart leading to heart failure. J Am Heart Assoc. 2013 May 20;2(3).

29. Cadenas S, Aragonés J, Landàzuri M O. Mitochondrial reprogramming through cardiac oxygen sensor in ischemic heart disease. Cardiovascular Research 2010; 88: 219-228.

30. Nabben M, Hoeks J. Mitochondrial uncoupling protein 3 and its role in cardiac- and skeletal muscle metabolism. Physiol Behav. 2008 23;94(2):259-69.

31. Stegger L, Schäfers K P, Flögel U, Lefteris L, Hermann S, Jacoby C, Keul P, Conway E M, Schiber O, Schrader J, Levkau B, Schäfers M. Monitoring Left Ventricular Dilation in Mice with PET. J Nucl Med 2005; 46: 1516-1521.

32. Stegger L,Heijman E, Schäfers K P, Nicolay K, Schäfers M A, Strijkers G J. Quantification of Left Ventricular Volumes and Ejection Fraction in mice using PET, compared with MRI. J Nucl Med 2009; 50:132-138.

33. Curcio A, Noma T, Naga Prasad SV, Wolf MJ, Lemaire A, Perrino C,

Mao L, Rockman HA. Competitive displacement of phosphoinositide 3-kinase from beta-adrenergic receptor kinase-1 improves postinfarction adverse myocardial remodeling. Am J Physiol Heart Circ Physiol. 2006;291:H1754-60.

34. Esposito G, Perrino C, Cannavo A, Schiattarella GG, Borgia F, Sannino A, Pironti G, Gargiulo G, Di Serafino L, Franzone A, Scudiero L, Grieco P, Indolfi C, Chiariello M. EGFR trans-activation by urotensin II receptor is mediated by beta-arrestin recruitment and confers cardioprotection in pressure overload induced cardiac hypertrophy. Basic Res Cardiol 2011;106:577-89.

35. Nekolla SG, Miethaner C, Nguyen N, Ziegler SI, Schwaiger M. Reproducibility of polar map generation and assessment of defect severity and extent assessment in myocardial perfusion imaging using positron emission tomography. Eur J Nucl Med 1998;25:1313-21.

36. Oh BH, Ono S, Rockman HA, Ross J Jr. Myocardial hypertrophy in the ischemic zone induced by exercise in rats after coronary reperfusion. Circulation 1993;87:598-607.

37. Ghesani M, Depuey EG, Rozanski A. Role of F-18 FDG positron emission tomography (PET) in the assessment of myocardial viability.

Echocardiography. 2005;22:165-77.

38. Lionetti V, Stanley WC, Recchia FA. Modulating fatty acid oxidation in heart failure. Cardiovasc Res. 2011;90:202-9

39. Echtay KS. Mitochondrial uncoupling proteins--what is their physiological role? Free Radic Biol Med. 2007;43:1351-71

40. Noma T, Nishiyama A, Mizushige K, Murakami K, Tsuji T, Kohno M, Rahman M, Fukui T, Abe Y, Kimura S. Possible role of uncoupling protein in regulation of myocardial energy metabolism in aortic regurgitation model rats. FASEB J. 2001;15:1206-8

41. Razeghi P, Myers TJ, Frazier OH, Taegtmeyer H. Reverse remodeling of the failing human heart with mechanical unloading. Emerging concepts and unanswered questions. Cardiology. 2002;98:167-74.

42. Brand MD, Esteves TC. Physiological functions of the mitochondrial uncoupling proteins UCP2 and UCP3. Cell Metab. 2005;2:85-93.

43. Laskowski KR, Russell RR 3rd. Uncoupling proteins in heart failure. Curr Heart Fail Rep. 2008;5:75-9.

44. Sochor H, Schelbert HR, Schwaiger M, Henze E, Phelps ME. Studies of fatty acid metabolism with positron emission tomography in

patients with cardiomyopathy. Eur J Nucl Med. 1986;12 Suppl:S66-9

45. Tadamura E, Kudoh T, Hattori N, Inubushi M, Magata Y, Konishi J, Matsumori A, Nohara R, Sasayama S, Yoshibayashi M, Tamaki N. Impairment of BMIPP uptake precedes abnormalities in oxygen and glucose metabolism in hypertrophic cardiomyopathy. J Nucl Med. 1998;39:390-6.

46. Dávila-Román VG, Vedala G, Herrero P, de las Fuentes L, Rogers JG, Kelly DP, Gropler RJ. Altered myocardial fatty acid and glucose metabolism in idiopathic dilated cardiomyopathy. J Am Coll Cardiol. 2002;40:271-7

47. de las Fuentes L, Herrero P, Peterson LR, Kelly DP, Gropler RJ, Dávila-RománVG. Myocardial fatty acid metabolism: independent predictor of left ventricular mass in hypertensive heart disease. Hypertension. 2003;41:83-7.

48. Remondino A, Rosenblatt-Velin N, Montessuit C, Tardy I, Papageorgiou I, Dorsaz PA, Jorge-Costa M, Lerch R. Altered expression of proteins of metabolic regulation during remodeling of the left ventricle after myocardial infarction. J Mol Cell Cardiol. 2000;32:2025-34.

49. Mailloux RJ, Dumouchel T, Aguer C, deKemp R, Beanlands R, Harper ME. Hexokinase II acts through UCP3 to suppress mitochondrial reactive oxygen species production and maintain aerobic respiration. Biochem J. 2011;437:301-11.

50. Rousset S, Alves-Guerra MC, Mozo J, Miroux B, Cassard-Doulcier AM, Bouillaud F, Ricquier D. The biology of mitochondrial uncoupling proteins. Diabetes. 2004;53 Suppl 1:S130-5

Table 1: Effects of genotype and myocardial infarction and their interaction on left ventricular volume at two-way analysis of variance

	Sum of square	**Degree of freedom**	**Mean square**	***F* value**	***P* value**
Model	1782	3	594	8.78	0.0003
Genotype	627	1	627	9.27	0.005
Myocardial infarction	805	1	805	11.9	0.002
Genotype/myocardial infarction	323	1	323	4.78	0.04
Residual	1826	27	68		
Total	3608	30	120		

Table 2: Effects of genotype and myocardial infarction and their interaction on SUV at two-way analysis of variance

	Sum of square	**Degree of freedom**	**Mean square**	***F* value**	***P* value**
Model	24	3	8.0	14.4	0.0001
Genotype	5.8	1	5.8	10.3	0.003
Myocardial infarction	12	1	12	21.6	0.0001
Genotype/myocardial infarction	5.4	1	5.4	9.79	0.004
Residual	15	27	0.56		
Total	39	30	1.30		

Figure 1

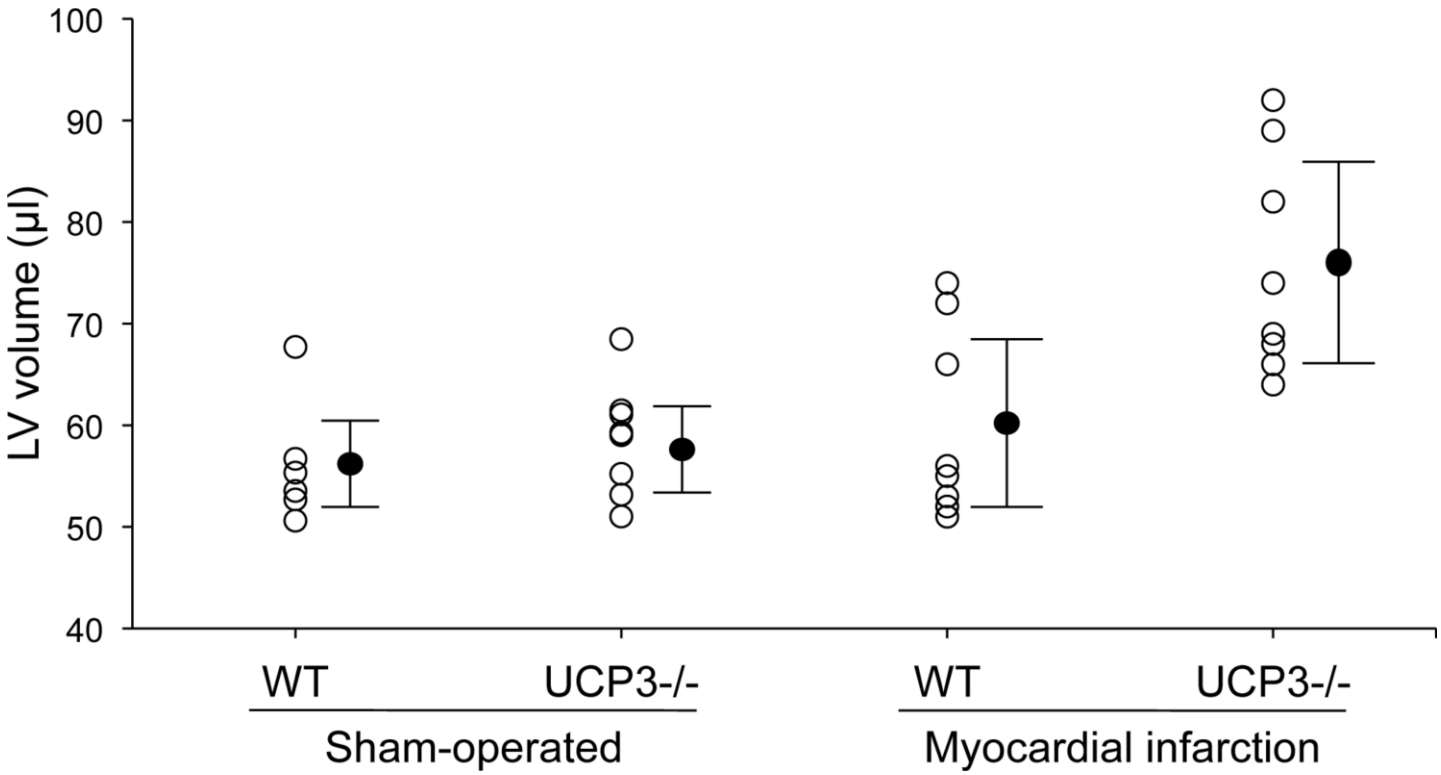

Individual values for LV volume in sham-operated and myocardial infarction WT and UCP3-/- mice. Closed circles indicate mean ± standard deviation.

Figure 2

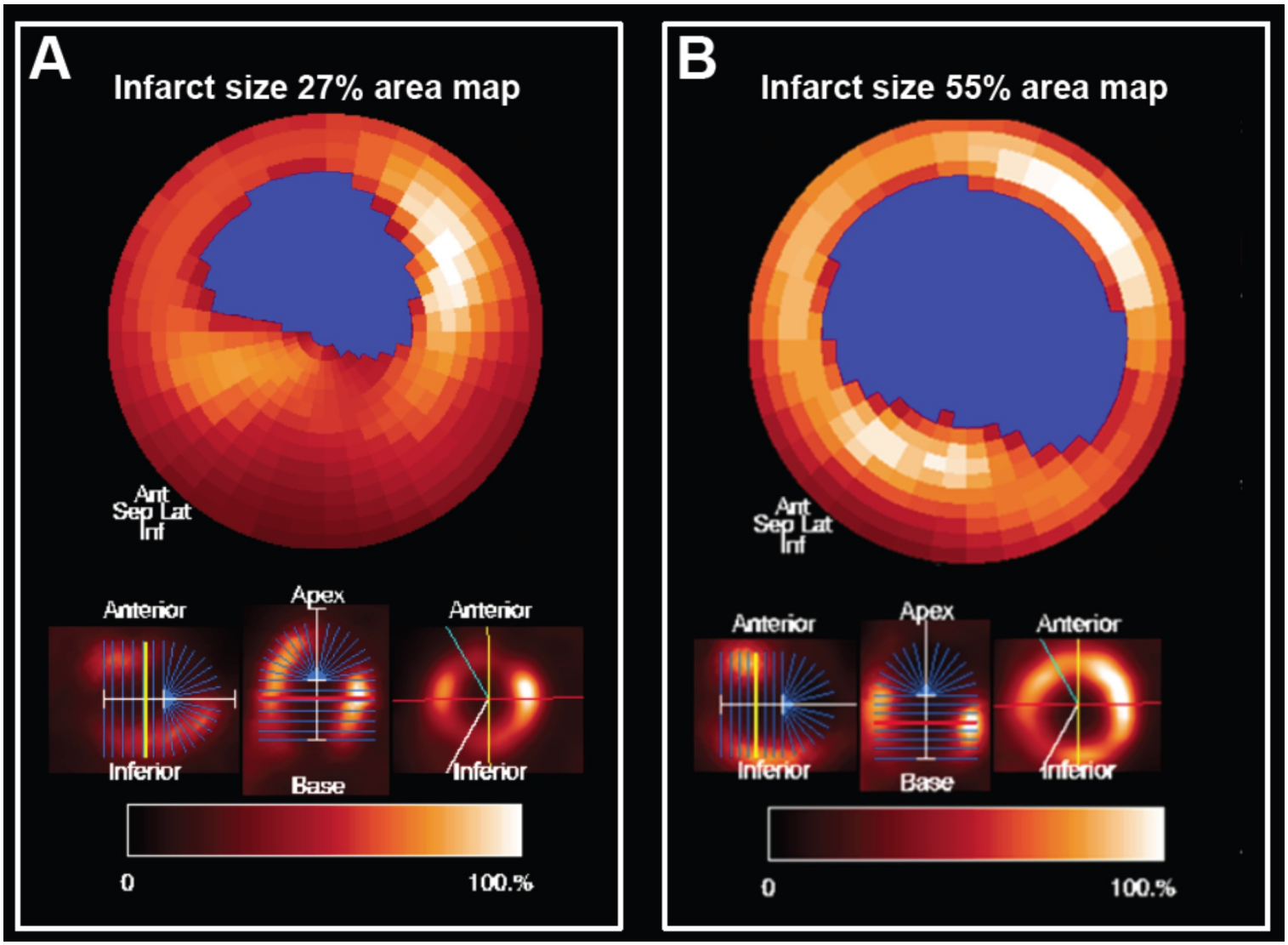

Vertical long-axis, horizontal long-axis, and short-axis slices (on the bottom) and the resulting polar map (on the top) in a WT mouse (A) and an UCP3-/- mouse (B) after myocardial infarction.

Figure 3

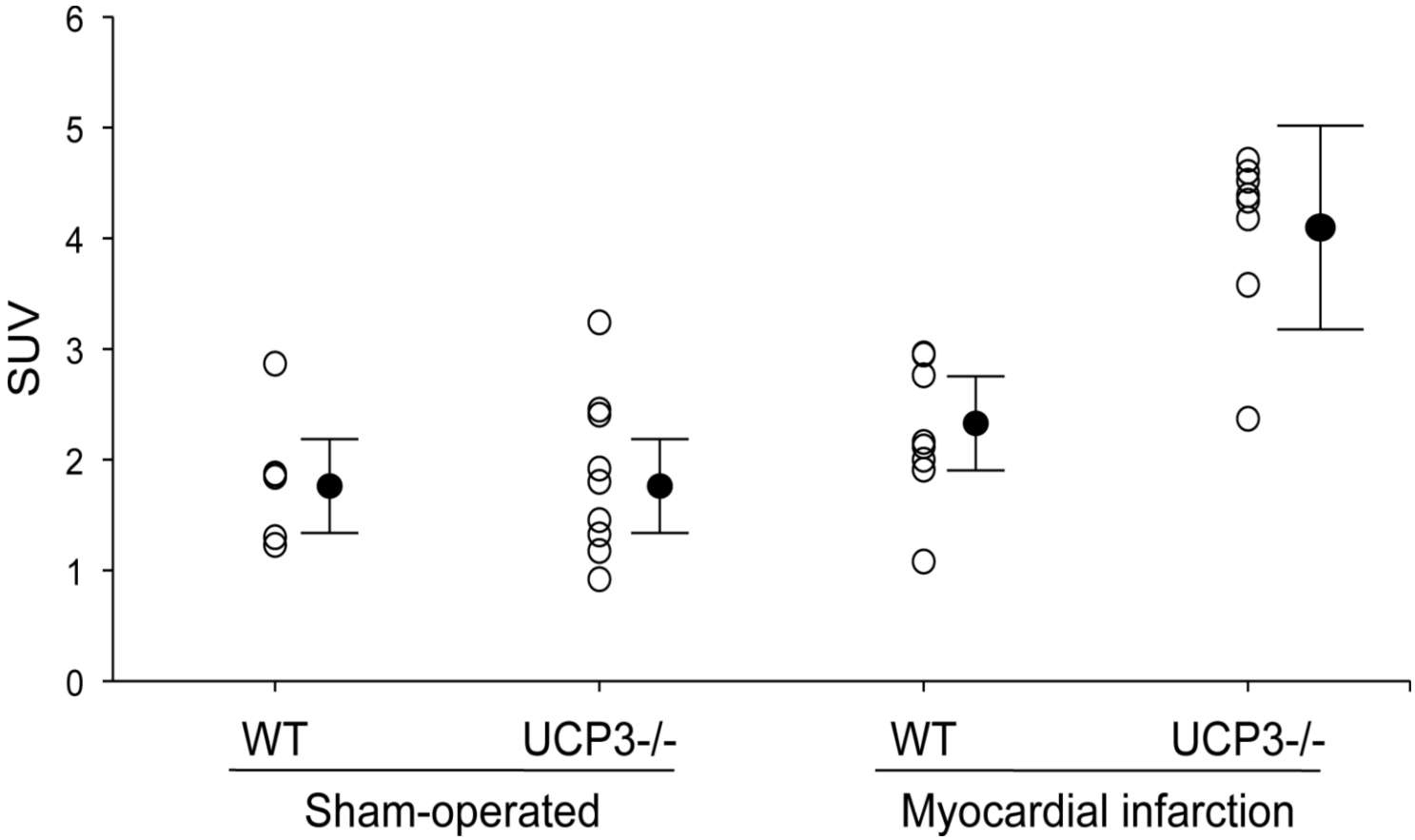

Individual values for SUV in sham-operated and myocardial infarction WT and UCP3-/- mice. Closed circles indicate mean ± standard deviation.

Figure 4

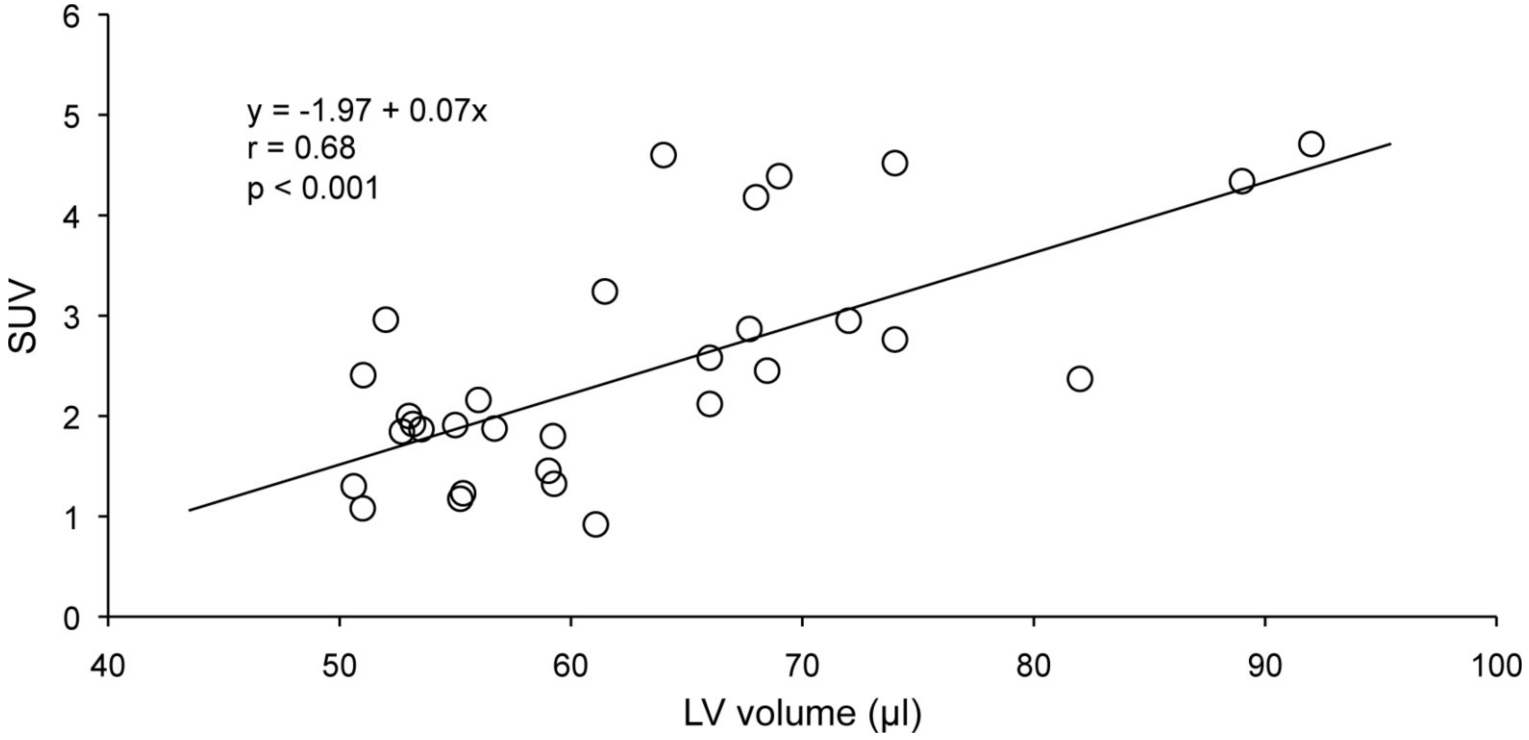

Relationship between LV volume and SUV at linear regression analysis.

Figure 5

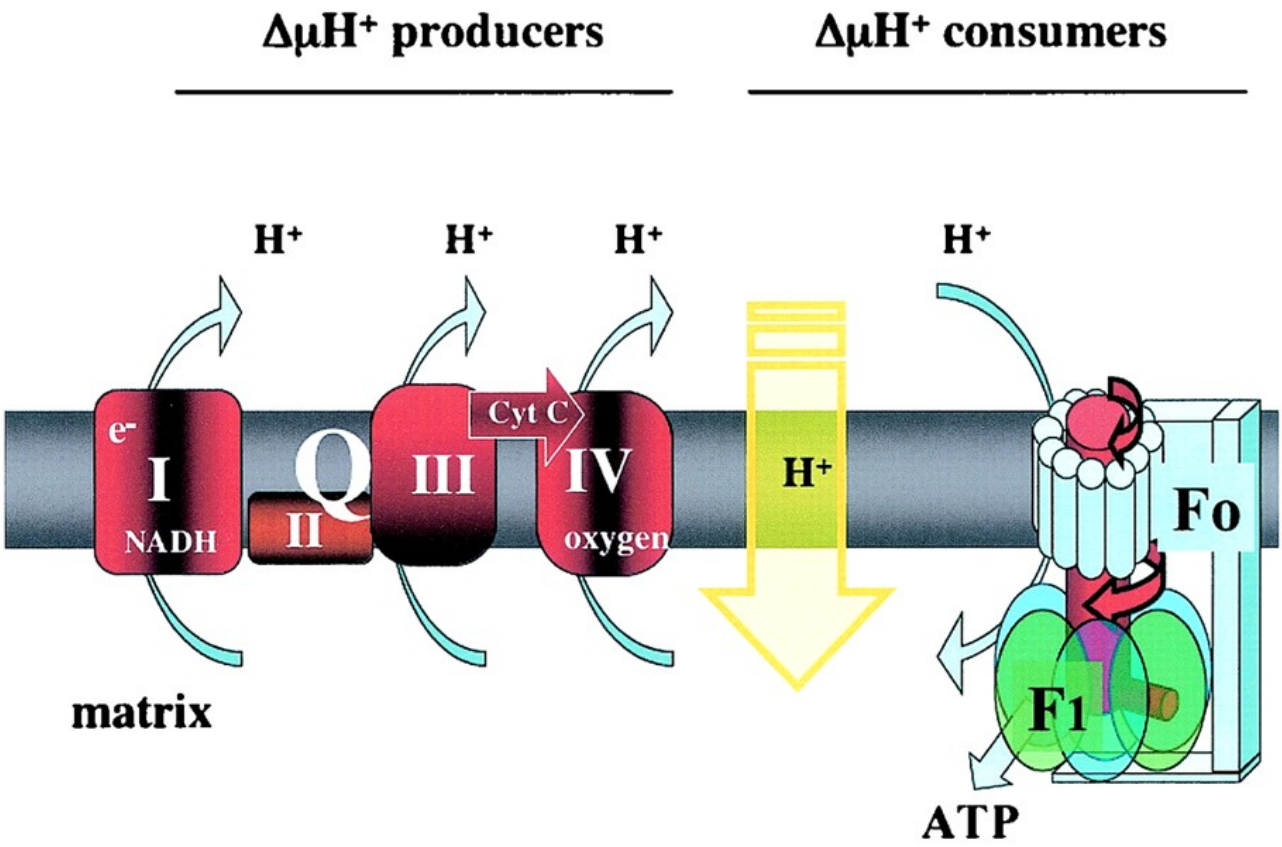

The mitochondrial proton gradient generated by complexes of respiratory chain is used by F0-F1-ATP synthase to phosphorylate ADP. Another mechanism consuming the gradient and lowering ATP synthesis is proton leak (yellow arrow). The reentry of protons in the matrix noncoupled with ATP synthesis is an energy-dissipating mechanism. The brown fat UCP1 is an example of mitochondrial proton leak. Cyt C, cytochrome C; H+, proton electrochemical gradient; e-, electron; F0: membranous part of ATP-synthase; F1: catalytic part of ATP-synthase.
(Adapted from "The Biology of Mitochondrial Uncoupling Proteins" Rousset S. et al. Diabetes. 2004;53 Suppl 1:S130-5.)